crystals

MDPI

Article

Synthesis and Characterization of the Amidomanganates $Rb_2[Mn(NH_2)_4]$ and $Cs_2[Mn(NH_2)_4]$

Christian Bäucker, Soeren Bauch and Rainer Niewa *

Institut für Anorganische Chemie, Universtität Stuttgart, Pfaffenwaldring 55, 70569 Stuttgart, Germany; baeucker@iac.uni-stuttgart.de (C.B.); soeren.bauch@online.de (S.B.)
* Correspondence: rainer.niewa@iac.uni-stuttgart.de

Abstract: We report the successful synthesis of $Rb_2[Mn(NH_2)_4]$ and $Cs_2[Mn(NH_2)_4]$ from ammonothermal conditions at 723 K and pressures above 850 bar. Both compounds were obtained single phase according to powder X-ray diffraction. The crystal structures were determined by single crystal X-ray diffraction. For $Rb_2[Mn(NH_2)_4]$ we have obtained the high-temperature phase. The structures are analyzed with respect to the earlier reported alkali metal amidomanganates. Upon heating in inert atmosphere $Cs_2[Mn(NH_2)_4]$ decomposes to manganese nitrides. IR spectroscopic results are reported.

Keywords: ammonothermal synthesis; amide; manganese

Citation: Bäucker, C.; Bauch, S.; Niewa, R. Synthesis and Characterization of the Amidomanganates $Rb_2[Mn(NH_2)_4]$ and $Cs_2[Mn(NH_2)_4]$. *Crystals* **2021**, *11*, 676. https://doi.org/10.3390/cryst11060676

Academic Editor: Volodymyr Bon

Received: 28 May 2021
Accepted: 9 June 2021
Published: 11 June 2021

1. Introduction

Ammonothermal synthesis is regarded as an innovative and promising approach for synthesis and growth of free-standing crystals of functional nitrides such as AlN [1], GaN [2] and InN [3] or other group III–V semiconductor materials [4]. Compared to further established methods such as chemical vapor deposition (CVD) it provides an alternative, less wasteful technique [5,6]. While the main interest in ammonothermal systems is fueled by the search for new or improved nitride semiconductors, transition metal amides are also widely available by this technique, such as Zn or Mn compounds [7,8]. These compounds are regarded as intermediates in the ammonothermal synthesis of transition metal nitrides like Zn_3N_2 [9] and Mn_3N_2 [10,11] and thus give a clue on the chemical processes during ammonothermal formation.

Ammonothermal synthesis is a derivative from the better known hydrothermal method, which share several common characteristics. Both methods typically use the supercritical fluid range, requiring temperatures above $T_c = 407.7$ K and pressures above $p_c = 119$ bar for ammonothermal systems [12]. Since ammonia is similar in behavior to water, the acidic and basic media as known in aqueous solutions can also be achieved in liquid ammonia by adding ammonobases such as alkali metal amides ANH_2 (A = Li – Cs) or ammonoacids such as ammonium halides NH_4X (X = F – I). The chemical nature of the intermediate and thus the solubility of any metal nitride and its temperature dependence are fundamentally affected by the nature of the mineralizer. While in an acidic milieu the product tends to precipitate in the colder zone of the autoclave, a basic milieu often causes products to crystallize in the hotter zone depending on the dissolved intermediate [13–16].

Recently, the successful synthesis of $K_2[Mn(NH_2)_4]$ and $Rb_2[Mn(NH_2)_4]$ by ball milling technique was reported [17]. Both compounds share the same chemical formula type as amidometalates like $K_2[Zn(NH_2)_4]$ [18], $Rb_2[Zn(NH_2)_4]$ [19] and $Cs_2[Zn(NH_2)_4]$ [8], these compounds well-known as intermediates in ammonothermal systems with zinc and ammonia. Thus, they give a deeper insight into the processes of dissolution and crystallization under ammonothermal conditions. Furthermore, the amidomanganates $Na_2[Mn(NH_2)_4]$ [7] and $K_2[Mn(NH_2)_4]$ [19] were previously obtained by reaction of the transition metal with a corresponding mineralizer in (supercritical) liquid ammonia. Generally, when heating

such amidometalates in inert atmosphere, a decomposition to the corresponding nitride is often observed, for example in the decomposition of $Rb[Al(NH_2)_4]$ to AlN [20].

In a previous report [17], two different modifications of $Rb_2[Mn(NH_2)_4]$ were observed, namely a low- and a high-temperature form. The low-temperature form with an orthorhombic structure in *Pbca* was obtained via ball-milling of rubidium and manganese under gaseous ammonia. Upon heating, this modification undergoes a phase transition to a monoclinic form in $P2_1/c$ at 429 K before starting to decompose. Generally, alkali metal amidometalates, such as $A_2[M(NH_2)_4]$ (A = Na – Cs, M = Mn, Zn) appear to be active in hydrogen storage and ammonia decomposition and formation [21], giving rise to useful applications. In this work, we describe the synthesis and crystal growth of the high-temperature modification of $Rb_2[Mn(NH_2)_4]$ as well as novel $Cs_2[Mn(NH_2)_4]$ from ammonothermal conditions and report crystal structures derived from single crystal X-ray diffraction, vibrational spectroscopy and thermal decomposition.

2. Materials and Methods

2.1. General Information

Due to air and moisture sensitivity, all handling of the starting materials and products was done in a glove box filled with argon (MBraun, Garching, Germany, $p(O_2) < 0.1$ ppm). Custom-made autoclaves (98 mL Volume, nickel-based alloy 718) [22] were used for reactions. One-side closed tubular furnaces (HTM Reetz GmbH, Berlin, Germany) caused a natural temperature gradient in the autoclave of about 100 K between the bottom and top of the reaction vessel. The different zones will be referred to as hot (bottom) and cold (top). Temperatures given at any point refer to the set temperature of the furnace, resulting in a lower actual temperature inside the autoclave, dependent on the one administered from outside [13]. To observe the maximum pressure inside the autoclave during the synthesis, the autoclave was fitted with a digital pressure transmitter (P2VA1/5000 and DA2510, HBM GmbH, Ismaning, Germany). In preparation, the starting materials were filled into the autoclave, which was then assembled, evacuated and flushed once with ammonia. Afterwards, ammonia was condensed into the reaction vessel using a dry-ice/ethanol cooling bath at approximately 200 K. NH_3 (99.999% anhydrous, Linde, Pullach, Germany) was purified from H_2O, CO_2 and O_2 to a grade less than one ppbV with the use of a MicroTorr MC400-720F gas purifier (Rainer Lammerz pure gas products, Hürth, Germany). A self-built tensi-eudiometer after Hüttig was used to precisely determine the amount of ammonia condensed into the autoclave [23].

Manganese powder (325 mesh, 99.95% metal basis, Alpha Aesar) was purchased and used as received. $RbNH_2$ and $CsNH_2$ were synthesized by reaction of the alkali metal in NH_3 at 383 K and 50 bar in 200 ml steel autoclaves (Carl Roth GmbH + Co. KG, Karlsruhe, Germany). The products were confirmed to be single phase by powder X-ray diffraction (PXRD).

2.2. Synthesis

$Rb_2[Mn(NH_2)_4]$ was synthesized from manganese powder and $RbNH_2$ with the following procedure: The autoclave was loaded with Mn (200.4 mg, 3.648 mmol) and $RbNH_2$ (741.1 mg, 7.302 mmol), filled with ammonia (2.13 mol) to a total of 54% volume and then heated to 723 K with a heating rate of 1.43 K/min reaching a maximum pressure of 880 bar. The autoclave was kept at this temperature for a duration of 24 h and then cooled down to room temperature with 0.149 K/min. The product was collected as yellow transparent crystalline plates from the hot zone of the autoclave. PXRD of the product shows no traces of residue $RbNH_2$.

$Cs_2[Mn(NH_2)_4]$ was obtained using the same procedure with manganese (154.3 mg, 2.809 mmol) and $CsNH_2$ (860.4 mg, 5.777 mmol) in ammonia (2.23 mol, 57% of total volume). A maximum pressure of p_{max} = 1150 bar was recorded. Again yellow plates crystallized in the hot zone were obtained.

2.3. Characterisation:

X-ray Diffraction: Single crystal X-ray diffraction data were measured on a Bruker-Nonius-Kappa-CCD with Mo$K_{\alpha 1}$ radiation (λ = 71.073 pm). The obtained data were processed using the program SHELX-97 [24]. Additional investigations on the micro-crystalline powder were performed on a STADI-P (STOE & Cie GmbH, Darmstadt, Germany) equipped with a Mythen 1-K detector and Mo$K_{\alpha 1}$ radiation. Visualisation of the resulting structures was done with the program Diamond 4.0 (Crystal Impact GbR, Bonn, Germany). Hydrogen positions could not be unambiguously located during the refinements. Since the exact location of hydrogen does not give deeper insights, also no riding model was applied.

Thermal Analysis: Investigations on thermal behaviour were conducted on a STA 449 C (NETZSCH GmbH, Selb, Germany) with an SiC furnace in corundum crucibles under continuous Argon flow (Argon 5.0, Air Liquide, Düsseldorf, Germany). Measurement data were analysed with the corresponding Proteus program package (Netzsch, Selb, Germany). The reaction chamber was evacuated and flushed with argon three times prior to any measurement, and a correction for buoyancy was administered.

Spectroscopy: Infrared spectroscopy measurements were performed on micro-crystalline powder samples on a Nicolet iS5 (Thermo Fischer Scientific, Waltham, MA, USA).

3. Results and Discussion

3.1. Crystal Structures of HT-$Rb_2[Mn(NH_2)_4]$ and $Cs_2[Mn(NH_2)_4]$

Yellow, plate-like crystals of $Rb_2[Mn(NH_2)_4]$ and $Cs_2[Mn(NH_2)_4]$ were obtained from manganese and the respective alkali metal amide in supercritical ammonia at a maximum temperature of 723 K and maximal pressures of 880 and 1150 bar, respectively. Both compounds were recovered from the hotter zone at the bottom of the autoclave interior, indicating a retrograde solubility, i.e., lower solubility at higher temperatures. While the cesium compound was not reported before, the crystals of $Rb_2[Mn(NH_2)_4]$ revealed the monoclinic unit cell of the high-temperature modification as reported by Cao et al. [17]. The unit cell volume of the well-crystallized product from high-pressure synthesis presents significantly larger than the one from ball-milling (740.86(4) $\times$ 10^6 pm^3 compared to 724.24(12) $\times$ 10^6 pm^3), despite the higher temperature during structure determination of the latter. Additionally, the high-temperature form did not undergo a structural transition to the low-temperature modification upon moderate heating up to 453 K, irrespective of the reported transition temperature of 429 K. The high-temperature form is thus either stabilized by the larger crystal size as compared to microcrystalline powder, or by deviations in composition. All discussed crystal structures contain mutually isolated tetraamidomanganate ions, however, arranged differently as shown in Figure 1. The difference in volumes of the differently synthesized samples of high-temperature rubidium tetraamidomanganate may indicate a deficiency of ammonia in the ball-milled sample, possibly via di- and oligomerization of the complex ions as was earlier observed for tetraamidoaluminates [20]. No reduced occupation of any sites were observed during the structure refinements against single crystal diffraction intensity data of the title compounds, while the structure of the high-temperature phase of $Rb_2[Mn(NH_2)_4]$ in literature was derived from temperature dependent powder diffraction data. Selected crystallographic data are gathered in Table 1. Fractional coordinates and isotropic displacement parameters are given in Table 2.

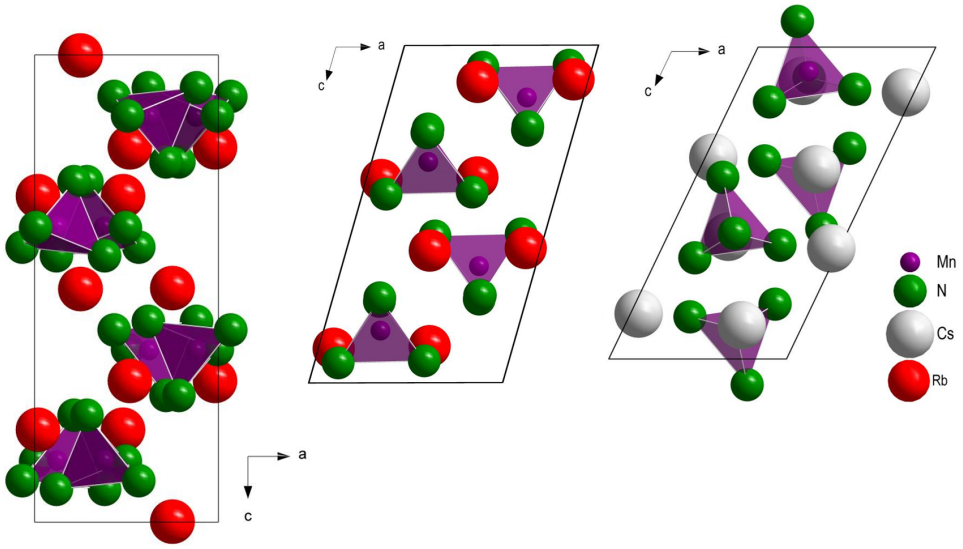

Figure 1. Unit cells of LT-$Rb_2[Mn(NH_2)_4]$ (**left**) [17], HT-$Rb_2[Mn(NH_2)_4]$ (**middle**) and $Cs_2[Mn(NH_2)_4]$ (**right**) with tetraamidomanganate ions shown as polyhedra. Viewing direction is $[0\bar{1}0]$.

Table 1. Selected crystallographic data and information concerning structure determination for HT-$Rb_2[Mn(NH_2)_4]$ and $Cs_2[Mn(NH_2)_4]$ from this work and comparison to literature data for the rubidium compound obtained from ball milling and subsequent phase transition from the respective low-temperature phase.

	Ref. [17]	**HT-$Rb_2[Mn(NH_2)_4]$**	**$Cs_2[Mn(NH_2)_4]$**
Crystal system	monoclinic	monoclinic	monoclinic
Space group	$P2_1/c$	$P2_1/c$	$P2_1/c$
a/pm	785.36(5)	779.45(3)	704.25(2)
b/pm	694.49(5)	702.04(2)	942.06(2)
c/pm	1384.11(11)	1408.48(5)	1396.04(4)
β/deg.	106.389(7)	106.004(2)	115.590(2)
$V/10^6$ pm^3	724.24(12)	740.86(4)	819.19(4)
Density/g cm^{-3}		2.600	3.121
Z		4	4
$F(000)$		540	684
hkl range		−10–9/−7–9/−16–18	±9/±12/±16
$2\Theta_{max}$/deg.		54.93	54.99
μ/mm^{-1}		14.74	10.29
Refl. meas./independent		12333/1690	21819/1876
$R_1/wR_2/GooF$		0.0489/0.1028/1.091	0.0369/0.0840/1.106
R_{int}/R_σ		0.0748/0.0375	0.0497/0.0192
Refined parameters		65	65
Extinction coefficient		0.00340	0.00614
$T_{measurement}$/K	429	293	293
Largest electron difference min/max/Å^{-3}		−0.70/0.67	−1.69/1.66

Table 2. Fractional coordinates and isotropic displacement parameters U_{eq} (in 10^4 pm^3) for HT-$Rb_2[Mn(NH_2)_4]$ and $Cs_2[Mn(NH_2)_4]$.

Atom	Wyckoff Site	*x*/*a*	*y*/*b*	*z*/*c*	U_{eq}
Rb(1)	4*e*	0.07762(6)	0.16605(7)	0.89877(4)	0.0412(2)
Rb(2)	4*e*	0.56877(6)	0.15528(7)	0.89187(3)	0.0399(2)
Mn	4*e*	0.70622(9)	0.19650(9)	0.65510(5)	0.0286(2)
N(1)	4*e*	0.4345(5)	0.2200(6)	0.5646(3)	0.0363(9)
N(2)	4*e*	0.8787(5)	0.2224(6)	0.5601(3)	0.0361(9)
N(3)	4*e*	0.7565(6)	0.0679(6)	0.2525(3)	0.0478(12)
N(4)	4*e*	0.2453(6)	0.0517(6)	0.2587(3)	0.0532(13)
Cs(1)	4*e*	0.04594(6)	0.03197(4)	0.35455(3)	0.0433(2)
Cs(2)	4*e*	0.34299(8)	0.15821(5)	0.10823(4)	0.0573(2)
Mn	4*e*	0.65076(13)	0.24799(9)	0.42175(7)	0.0325(2)
N(1)	4*e*	0.6317(8)	0.0223(5)	0.4028(4)	0.0401(11)
N(2)	4*e*	0.7880(9)	0.1695(7)	0.8243(5)	0.0558(15)
N(3)	4*e*	0.3435(9)	0.1677(6)	0.8648(5)	0.0565(15)
N(4)	4*e*	0.8481(9)	0.1940(6)	0.0827(5)	0.0507(13)

For $Cs_2[Mn(NH_2)_4]$ a closer inspection of the packing concerning the $[Mn(NH_2)_4]^{2-}$ complex anions reveals the motif of hexagonal closest packing along [010] (see Figure 2), also known from the isotypes $Cs_2[Mg(NH_2)_4]$ [25] and $Cs_2[Zn(NH_2)_4]$ [8]. HT-$Rb_2[Mn(NH_2)_4]$ is an isotype of $A_2[Mg(NH_2)_4]$ with A = K, Rb [26], $A_2[Zn(NH_2)_4]$ with A = K, Rb [18,19], and $K_2[Mn(NH_2)_4]$ [19]. Here, the tetraamidometalate ions similarly realize a hexagonal closest packing along [010], but strongly distorted.

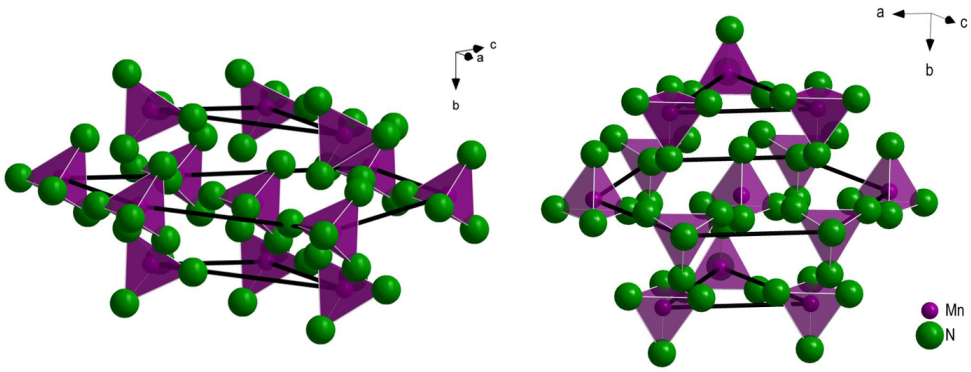

Figure 2. Representations of the motifs of hexagonal closest packings formed by the complex anions in HT-$Rb_2[Mn(NH_2)_4$ (**left**) and $Cs_2[Mn(NH_2)_4]$ (**right**). The alkali metal cations are omitted for clarity.

In HT-$Rb_2[Mn(NH_2)_4]$ the rubidium ions of both crystallographically distinct sites exhibit nearly identical eight-fold (7 + 1) coordination environments of amide groups with the shape of two-capped trigonal prisms. The larger cesium cations in $Cs_2[Mn(NH_2)_4]$ realize larger polyhedra with nine and eleven amide groups surrounding Cs(1) and Cs(2), respectively. Selected interatomic distances and angles are gathered in Table 3.

Table 3. Selected bond distances (in pm) and angles (in deg.) in HT-$Rb_2[Mn(NH_2)_4]$ and $Cs_2[Mn(NH_2)_4]$.

Distance	$Rb_2[Mn(NH_2)_4]$		$Cs_2[Mn(NH_2)_4]$		Angle	$Rb_2[Mn(NH_2)_4]$	$Cs_2[Mn(NH_2)_4]$
	Rb(1)	Rb(2)	Cs(1)	Cs(2)			
A–N	316.9(4)	300.5(4)	315.2(5)	333.5(7)	N(1)–Mn–N(2)	107.542(2)	108.174(1)
	318.2(4)	303.0(4)	325.9(5)	336.6(6)	N(1)–Mn–N(3)	107.435(1)	109.152(1)
	320.1(4)	311.8(4)	327.5(6)	344.1(5)	N(1)–Mn–N(4)	113.428(1)	111.297(1)
	322.9(5)	319.0(4)	329.8(6)	346.0(6)	N(2)–Mn–N(3)	107.734(1)	107.763(1)
	324.2(5)	322.6(5)	348.7(6)	363.3(7)	N(2)–Mn–N(4)	112.875(1)	106.921(1)
	330.9(5)	336.9(5)	360.1(6)	370.6(6)	N(3)–Mn–N(4)	107.558(1)	113.329(1)
	334.0(4)	339.1(5)	366.6(6)	373.7(6)			
	395.1(1)	401.3(1)	369.4(6)	386.7(6)			
			388.7(6)	387.6(7)			
				407.5(1)			
				415.6(1)			
Mn–N(4)	209.8(4)		210.7(5)				
Mn–N(3)	211.6(4)		211.3(5)				
Mn–N(2)	215.0(4)		210.5(6)				
Mn–N(1)	215.6(4)		213.9(5)				

For both title compounds, the coordination polyhedra surrounding the alkali metal ions connect to columns. In HT-$Rb_2[Mn(NH_2)_4]$ the monocapped trigonal prisms share the triangular faces, resulting in straight columns parallel to the *a*-axis as shown in Figure 3. These columns are further connected via edge-sharing to form a three-dimensional framework hosting the manganese ions in tetrahedral voids of the amide groups. In $Cs_2[Mn(NH_2)_4]$ instead a three-dimensional network of polyhedra around the cesium sites, connected by face-, edge- and corner-sharing is realized. Similar to the rubidium compound, the manganese is found in tetrahedral voids (see Figure 3).

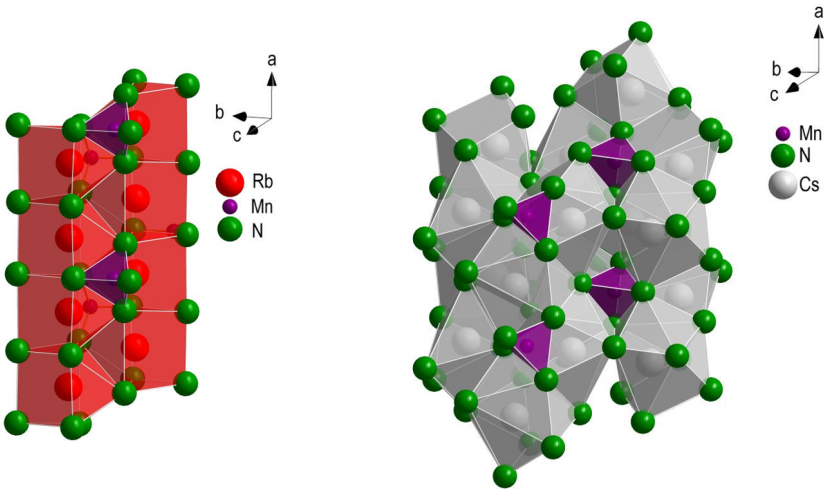

Figure 3. Interconnection of polyhedra surrounding the alkali metal ions in HT-$Rb_2[Mn(NH_2)_4]$ (**left**) and $Cs_2[Mn(NH_2)_4]$ (**right**).

3.2. Comparison of Structures of Known Alkali Metal Amidomanganates

Currently five structure types for alkali metal amidometalates with the composition $A_2[M(NH_2)_4]$ and *A* = Na – Cs, *M* = Mg, Mn, Zn are known. As expected, the coordination number of the alkali metal ions with respect to amide ions monotonically increase from six for sodium up to eleven for cesium. Particularly for $Rb_2[Mn(NH_2)_4]$, a low- and a high-temperature modification are known. In the high-temperature title phase, all rubidium ions are coordinated by only eight amide ions, while in the low-temperature phase they are surrounded by eight or nine amide groups [17]. Noteworthy, all structure types contain two crystallographic sites for the alkali metal ion. It is interesting to compare the coordination environments in the isostructural compounds $K_2[M(NH_2)_4]$ with those of HT-$Rb_2[M(NH_2)_4]$, both with *M* = Mg, Mn, Zn: In the potassium compounds, the coordination

is best described as seven-fold, while due to the increased size of the rubidium ions and a shorter relative distance, one additional amide edge of a coordination polyhedron must be taken into account for both alkali metal sites.

As recently demonstrated for the three modifications of $Ba[Ga(NH_2)_4]_2$, which all realize coordination environments with eight amide groups for the barium ions, differences in coordination behaviour can be effectively described by extending the cation environments with the full tetrahedral $[Mn(NH_2)_4]^{2-}$ complex anions [27]. In Figure 4, all these coordination environments are gathered. The full $[Mn(NH_2)_4]^{2-}$ ions are shown, if they coordinate by two or three amide groups. If connected to the central alkali metal atom only by one amide group, the tetrahedral complex ion is omitted for clarity. A clear difference in local structures is found in the arrangements of the type of complex $[Mn(NH_2)_4]^{2-}$ ions in the coordination of the alkali metal ions. With increasing alkali metal size, not only the coordination number increases, but in general, also the number of different complex ions in the direct neighborhood and particularly the number of bi- and tridentate coordinations of those. In $Na_2[Mn(NH_2)_4]$ [7], two monodentate and two bidentatete tetrahedra are attached to each crystallographically distinct sodium ion in very similar arrangements. The triclinic form of $K_2[Zn(NH_2)_4]$ [18], for which no manganese representative is known so far, realizes qualitatively the same situation on one potassium ion, while the second one interestingly carries only one bidentate complex ion but three monodentate ones. Since $K_2[Mn(NH_2)_4]$ and the HT-$Rb_2[Mn(NH_2)_4]$ both share the same crystal structure [19], the surrounding of the alkali metals is similar, but in HT-$Rb_2[Mn(NH_2)_4]$ extended to a coordination with three bi- and two monodentate tetrahedra ligands on one and already four bidentate ligands at the second rubidium ion. However, the LT-form of $Rb_2[Mn(NH_2)_4]$ already exhibits a tridentate connection additionally two bi- and one monodentate ones for one alkali metal site, while the other is still attached to three bidentate and two monodentate tetrahedra [17]. Lastly, in $Cs_2[Mn(NH_2)_4]$, the Cs(1) site exhibits a total of three tetrahedra connecting bi- and three monodentate. The Cs(2) site even is coordinated by two three-, two bi- and only one monodentate tetrahedra.

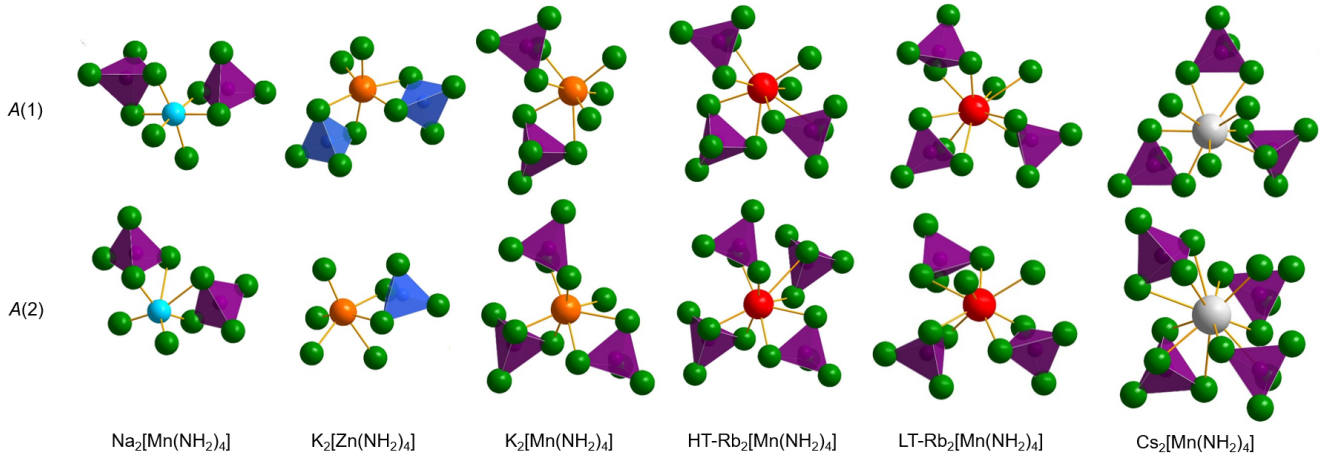

Figure 4. Different coordination environments of alkali metal sites in $A_2[Mn(NH_2)_4]$ (A = Na – Cs) and $K_2[Zn(NH_2)_4]$ [7,17–19], the A(1) site is shown in the top row, A(2) below. Manganese is pictured in purple, zinc in dark blue and nitrogen in green. $[M(NH_2)_4]^{2-}$ tetrahedra only coordinating via one amide group are omitted for clarity.

3.3. Vibrational Spectroscopy

While Raman spectroscopy proved difficult due to decomposition, measurements with infrared radiation posed possible for both HT-$Rb_2[Mn(NH_2)_4]$ and $Cs_2[Mn(NH_2)_4]$. HT-$Rb_2[Mn(NH_2)_4]$ shows four signals in total in between 3217 and 3342 cm^{-1}, which can be assigned to NH_2^- valence vibrations ν(N–H), in agreement with two groups of amide ions with very similar surroundings each in the crystal structure. Signals in the range of 1516–1549 cm^{-1} can be assigned to amide deformation modes δ(H–N–H). Further signals below 600 cm^{-1} are probably caused by Mn–N lattice vibrations. Since these are numerous and ambiguous to assign, they were omitted from Table 4.

For $Cs_2[Mn(NH_2)_4]$, IR bands can be found within the same ranges: ν(N–H) = 3236–3297 cm^{-1}, δ(H–N–H) = 1525–1538 cm^{-1}. Due to even more similar environments of the four distinct amide groups, we observed only three valence modes compared to the rubidium compound as well as only two deformation modes.

All assignments of signals were done in accordance to data on similar compounds like $NaNH_2$, $Rb[Al(NH_2)_4]$, $Cs[Al(NH_2)_4]$ and $Cs_2[Zn(NH_2)_4]$ [8,28,29].

Table 4. List of observed modes in the infrared spectra of HT-$Rb_2[Mn(NH_2)_4]$ and $Cs_2[Mn(NH_2)_4]$. All values are given in cm^{-1}.

	HT-$Rb_2[Mn(NH_2)_4]$	**$Cs_2[Mn(NH_2)_4]$**
Valence modes		
	3342	3297
	3327	3248
	3275	3236
	3217	
Bending modes		
	1549	1538
	1529	1525
	1516	

3.4. Thermal Analysis

Thermal decomposition of $Cs_2[Mn(NH_2)_4]$ was performed in inert atmosphere. The thermal gravimetry (TG) curve shows a total of three steps of decomposition. Similar to the decomposition of other amidometalates such as $Na[Al(NH_2)_4]$ or $Rb[Al(NH_2)_4]$ [20,30], ammonia is first released from the compound (3.8% of total mass) starting at a temperature of about 370 K. The difference to the expected weight loss of 5.9% for 4/3 equivalents of ammonia per formula unit might be explained with premature decomposition during evacuation of the thermal analyzer in order to remove air and humidity prior to filling with argon gas for measurement. In a second step of 56.1%, $CsNH_2$ evaporates (expected 77.4%). In a third and final step, manganese nitride Mn_3N_2 decomposes and manganese slowly evaporates, leaving traces of manganese oxide behind. The TG curve is shown in Figure 5. Contrary to observations of Cao et al. in the decomposition of $Rb_2[Mn(NH_2)_4]$, $CsNH_2$ could not be identified after the first decomposition step at about 573 K by powder X-ray diffraction [17]. Instead, reflections were assigned to manganese oxide, MnO, and the manganese nitrides Mn_3N_2 and Mn_4N next to unknown phases. Upon further decomposition at higher temperatures, the signals due to Mn_3N_2 gradually disappear.

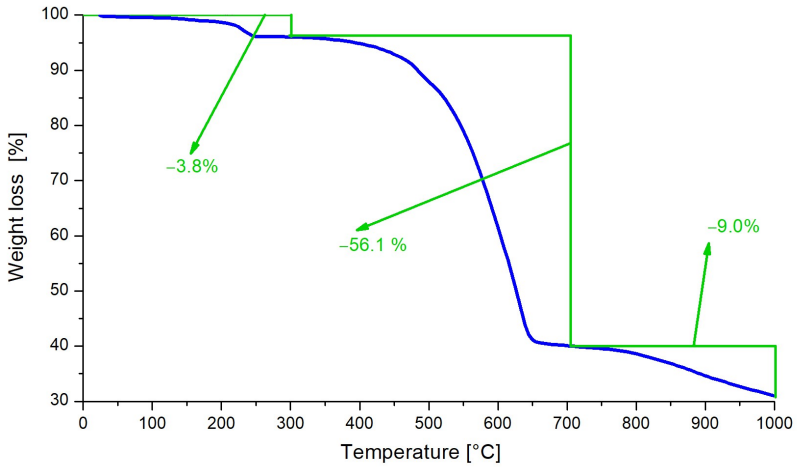

Figure 5. TG measurement of $Cs_2[Mn(NH_2)_4]$ at 5 K/min in argon flow. Proposed decomposition steps have been added to the figure together with measured percentage mass loss.

4. Conclusions

The successful synthesis and crystal growth of HT-$Rb_2[Mn(NH_2)_4]$ and $Cs_2[Mn(NH_2)_4]$ by ammonothermal method is reported. The structures of those compounds fit smoothly into the structural evolution of the known alkali metal amidomanganates(II) and related amidometalates(II) of Mg and Zn. The atomic arrangements exhibit rising coordination numbers and multidentate coordination of tetraamidometalate ions at the alkali metal ions with increasing radius. The amidomanganates expectedly produce binary manganese nitrides upon decomposition in inert atmosphere.

Author Contributions: Conceptualization, C.B. and R.N.; methodology, C.B.; validation, C.B. and R.N.; formal analysis, C.B. and S.B.; investigation, C.B. and S.B.; resources, R.N.; data curation, C.B. and S.B.; writing—original draft preparation, C.B.; writing—review and editing, R.N.; visualization, C.B. and R.N.; supervision, R.N.; project administration, R.N.; funding acquisition, R.N. All authors have read and agreed to the published version of the manuscript.

Funding: This research was funded by the German Research Foundation (DFG) within grant number NI489/16-1.

Data Availability Statement: Supplementary crystallografic data can be obtained online free of charge via http://www.ccdc.cam.ac.uk/conts/retrieving.html (accessed on 28 May 2021), depositon numbers CSD 2084385 ($Rb_2[Mn(NH_2)_4]$) and 2084386 ($Cs_2[Mn(NH_2)_4]$).

Acknowledgments: We thank Sebastian Kunkel and Florian Goerigk for recording vibriational spectra. Furthermore, funding by the DFG via grand NI489/16-1 is greatly acknowledged.

Conflicts of Interest: The authors declare no conflict of interest.

References

1. Lan, Y.C.; Chen, X.L.; Cao, Y.G.; Xu, Y.P.; Xun, L.D.; Xu, T.; Liang, J.K. Low-temperature synthesis and photoluminescence of AlN. *J. Cryst. Growth* **1999**, *207*, 247–250. [CrossRef]
2. Dwiliński, R.; Baranowski, J.M.; Kamińska, M.; Doradziński, R.; Garczyński, J.; Sierzputowski, L. On GaN crystallization by ammonothermal method. *Acta Phys. Pol. A* **1996**, *90*, 763–766. [CrossRef]
3. Hertrampf, J.; Becker, P.; Widenmeyer, M.; Weidenkaff, A.; Schlücker, E.; Niewa, R. Ammonothermal Crystal Growth of Indium Nitride. *Cryst. Growth Des.* **2018**, *18*, 2365–2369. [CrossRef]
4. Richter, T.M.M.; Niewa, R. Chemistry of Ammonothermal Synthesis. *Inorganics* **2014**, *2*, 29–78. [CrossRef]
5. Maruska, H.Á.P.; Tietjen, J.J. The preparation and properties of vapor-deposited single-crystalline GaN. *Appl. Phys. Lett.* **1969**, *15*, 327–329. [CrossRef]
6. Tietjen, J.J.; Amick, J.A. The preparation and properties of vapor-deposited epitaxial $GaAs_{1-x}P_x$ using arsine and phosphine. *J. Electrochem. Soc.* **1966**, *113*, 724–728. [CrossRef]
7. Fröhling, B.; Jacobs, H. $Na_2[Mn(NH_2)_4]$: Ein neuer Schichtenstrukturtyp. *Z. Anorg. Allg. Chem.* **1997**, *623*, 1108–1112. [CrossRef]

8. Richter, T.M.M.; Alt, N.S.A.; Schlücker, E.; Niewa, R. Ammonothermal Synthesis and Characterization of $Cs_2[Zn(NH_2)_4]$. *Z. Anorg. Allg. Chem.* **2016**, *642*, 1207–1211. [CrossRef]
9. Richter, T.M.M.; Strobel, S.; Alt, N.S.A.; Schlücker, E.; Niewa, R. Ammonothermal Synthesis and Crystal Structures of Diammine-triamidodizinc Chloride $[Zn_2(NH_3)_2(NH_2)_3]Cl$ and Diamminemonoamidozinc Bromide $[Zn(NH_3)_2(NH_2)]Br$. *Inorganics* **2016**, *4*, 41. [CrossRef]
10. Kreiner, G.; Jacobs, H. Magnetische Struktur von η-Mn_3N_2. *J. Alloys Compd.* **1992**, *183*, 345–362. [CrossRef]
11. Jacobs, H.; Stüve, C. Hochdrucksynthese der η-phase im System Mn-N: Mn_3N_2. *J. Less Common Met.* **1984**, *96*, 323–329. [CrossRef]
12. Juza, R.; Jacobs, H.; Gerke, H. Ammonothermalsynthese von Metallamiden und Metallnitriden. *Ber. Bunsenges. Phys. Chem.* **1966**, *70*, 1103–1105. [CrossRef]
13. Zhang, S. Intermediates during the Formation of GaN under Ammonothermal Conditions. Doctoral Thesis, University of Stuttgart, Stuttgart, Germany, 2014.
14. Wang, B.; Callahan, M.J. Transport growth of GaN crystals by the ammonothermal technique using various nutrients. *J. Cryst. Growth* **2006**, *291*, 455–460. [CrossRef]
15. Peters, D. Ammonothermal synthesis of aluminum nitride. *J. Cryst. Growth* **1990**, *104*, 411–418. [CrossRef]
16. Wang, B.; Callahan, M.; Rakes, K.; Bouthillette, L.; Wang, S.Q.; Bliss, D.; Kolis, J. Ammonothermal growth of GaN crystals in alkaline solutions. *J. Cryst. Growth* **2006**, *287*, 376–380. [CrossRef]
17. Cao, H.; Guo, J.; Chang, F.; Pistidda, C.; Zhou, W.; Zhang, X.; Santoru, A.; Wu, H.; Schell, N.; Niewa, R.; et al. Transition and Alkali Metal Complex Ternary Amides for Ammonia Synthesis and Decomposition. *Chem. Eur. J.* **2017**, *23*, 9766–9771. [CrossRef]
18. Richter, T.M.M.; Zhang, S.; Niewa, R. Ammonothermal synthesis of dimorphic $K_2[Zn(NH_2)_4]$. *Z. Kristallogr. Cryst. Mater.* **2013**, *228*, 351–358. [CrossRef]
19. Drew, M.; Guémas, L.; Chevalier, P.; Palvadeau, P.; Rouxel, J. Etude structurale de l'amidozincate de rubidium $Rb_2Zn(NH_2)_4$ et de l'amidomanganite de potassium $K_2Mn(NH_2)_4$. *Rev. Chim. Min.* **1975**, *12*, 419–426.
20. Bäucker, C.; Niewa, R. A New Modification of $Rb[Al(NH_2)_4]$ and Condensation in Solid State. *Crystals* **2020**, *10*, 1018. [CrossRef]
21. Cao, H.; Santoru, A.; Pistidda, C.; Richter, T.M.; Chaudhary, A.L.; Gizer, G.; Niewa, R.; Chen, P.; Klassen, T.; Dornheim, M. New synthesis route for ternary transition metal amides as well as ultrafast amide–hydride hydrogen storage materials. *Chem. Commun.* **2016**, *52*, 5100–5103. [CrossRef]
22. Alt, N.S.A.; Meissner, E.; Schluecker, E. Development of a novel in situ monitoring technology for ammonothermal reactors. *J. Cryst. Growth* **2012**, *350*, 2–4. [CrossRef]
23. Hüttig, G.F. Apparat zur gleichzeitigen Druck- und Raummessung von Gasen.(Tensi-Eudiometer.). *Z. Anorg. Allg. Chem.* **1920**, *114*, 161–173. [CrossRef]
24. Sheldrick, G.M. Crystal structure refinement with *SHELXL*. *Acta Crystallogr. C* **2015**, *71*, 3–8. [CrossRef] [PubMed]
25. Jacobs, H.; Birkenbeul, J.; Schmitz, D. Strukturverwandtschaft des Dicaesiumamidomagnesats, $Cs_2[Mg(NH_2)_4]$, zum β-K_2SO_4-Typ. *J. Less Common Met.* **1982**, *85*, 79–86. [CrossRef]
26. Jacobs, H.; Birkenbeul, J.; Kockelkorn, J. Darstellung und Eigenschaften der Amidomagnesate des Kaliums und Rubidiums $K_2[Mg(NH_2)_4]$- und $Rb_2[Mg(NH_2)_4]$-Verbindungen mit isolierten $[Mg(NH_2)_4]^{2-}$-Tetraedern. *J. Less Common Met.* **1984**, *97*, 205–214. [CrossRef]
27. Hertrampf, J.; Alt, N.S.A.; Schlücker, E.; Niewa, R. Three Solid Modifications of $Ba[Ga(NH_2)_4]_2$: A Soluble Intermediate in Ammonothermal GaN Crystal Growth. *Eur. J. Inorg. Chem.* **2017**, *2017*, 902–909. [CrossRef]
28. Liu, A.; Song, Y. In Situ High-Pressure Study of Sodium Amide by Raman and Infrared Spectroscopies. *J. Phys. Chem. B* **2011**, *115*, 7–13. [CrossRef] [PubMed]
29. Jacobs, H.; Jänichen, K. Darstellung und Kristallstruktur von Tetraamidoaluminaten des Rubidiums und Caesiums. *J. Less Common Met.* **1990**, *159*, 315–325. [CrossRef]
30. Jacobs, H.; Nöcker, B. Neubestimmung von Struktur und Eigenschaften isotyper Natriumtetraamidometallate des Aluminiums und Galliums. *Z. Anorg. Allg. Chem.* **1993**, *619*, 381–386. [CrossRef]